Chemical Physics Impact 7 (2023) 100373

Contents lists available at ScienceDirect

Chemical Physics Impact

journal homepage: www.sciencedirect.com/journal/chemical-physics-impact

Full Length Article

Assessments of carbon and boron nitride graphdiyne nanosheets for exploring the amphetamine drug adsorbents/sensors along with density functional theory

M.J. Saadh [a], S.M. Mohealdeen [b], C.Y. Hsu [c], U.A. Jumanazarov [d], R.R. Maaliw III [e], M. Mirzaei [f], M. Da'i [g], K. Harismah [h,*]

[a] Faculty of Pharmacy, Middle East University, Amman 11831, Jordan
[b] Department of Radiology & Sonar Techniques, Al-Noor University College, Nineveh, Iraq
[c] Department of Pharmacy, Chia Nan University of Pharmacy and Science, Tainan, Taiwan
[d] Jizzakh State Pedagogical University, Jizzakh, Uzbekistan
[e] College of Engineering, Southern Luzon State University, Lucban, Quezon, Philippines
[f] Laboratory of Molecular Computations (LMC), Department of Natural and Mathematical Sciences, Faculty of Engineering, Tarsus University, Tarsus, Turkey
[g] Faculty of Pharmacy, Universitas Muhammadiyah Surakarta, Surakarta, Indonesia
[h] Department of Chemical Engineering, Faculty of Engineering, Universitas Muhammadiyah Surakarta, Surakarta, Indonesia

ARTICLE INFO

Keywords:
Adsorbent
Emergency detection
Molecular interaction
Quantum calculations
Sensor

ABSTRACT

By the importance of developing detection materials and devices, the current work was done to provide molecular insights into the exploration of amphetamine (AMP) adsorbents/sensors through the density functional theory (DFT) assessments of carbon (g-C) and boron nitride (g-BN) graphdiyne nanosheets. Since AMP could be very harmful in an overdose level, then its careful detection is very important for employing the appropriate emergency cares and activities. The optimization calculations were performed to stabilize the structures of singular models and their corresponding AMP@g-C and AMP@g-BN complex, in which a higher strength was found for the formation AMP@g-C complex. Bothe complexes were stable enough to be recognized based on their formations and also by monitoring the variations of frontier molecular orbital features. The results indicated that the formation of AMP@g-BN complex could be used for an immediately detection whereas the formations of AMP@g-C complex could be used for a timely detection. Both complexes were found reusable based on the formation of non-covalent interactions between the substances, in which the stabilities and molecular orbitals features proposed both of g-C and g-BN nanosheets as suitable adsorbent/sensor materials of AMP substance for developing novel detection materials and devices.

1. Introduction

Sensors are very important devices/materials for working in different purposes including detection and removal functions of especially traceless and low-concentration substances regarding the material science developmental issues [1–3]. On the other hand, they could also push forward several electronic activities and energy storages for approaching the purposes of engineering issues [4–6]. Hence, sensors are very important to be developed more and more to supply the needs of science and engineering in the modern life [7–9]. Indeed, the surface of an appropriate adsorbent could manage the sensing function to work in the specific functions and applications regarding the adsorption or sensor purposes [10–12]. For the case of detection, the sensor devices are very useful to sense the existence of any toxic substance regarding the health and environmental issues [13–15]. In this regard, the consumption of some forbidden drug substances or their overdosing should be detected in a short time for providing required emergency cares [16–18]. Amphetamine; or 1-phenylpropan-2-amine, is one of those drugs with therapeutic functions but an unauthorized and abnormal consumption could lead to the appearance of significant health risks [19–21]. Amphetamine stimulates the central nervous system (CNS) for treating some types of psychological disorders such as attention deficit hyperactivity disorder (ADHD), narcolepsy, and obesity [22–24]. Additionally, an athletic performance could be enhanced under the

* Corresponding author.
E-mail address: kun.harismah@ums.ac.id (K. Harismah).

https://doi.org/10.1016/j.chphi.2023.100373
Received 15 October 2023; Received in revised form 5 November 2023; Accepted 5 November 2023
Available online 7 November 2023

consumption of amphetamine in addition to the enhancement of cognition and recreation in a better emotional mood [25–27]. Besides the positive impacts of low therapeutic dosages, larger dosages of amphetamine or addiction could lead to cognition and muscle failures as serious psychosis and abnormal physical behavior risks [28–30]. Because of very serious negative impacts of an uncontrolled consumption of amphetamine, its detection should be done in an earliest time for employing the required emergency activities to keep the human life [31–33]. Hereby, considerable efforts have been devoted to explore convenient sensors towards the detection of amphetamine especially by the exhaled breathing air [34–36]. To this point, providing a precise adsorbent/sensor material could help to approach a fast detection process regarding the importance of subsequent activities [37–39]. Accordingly, the topic of current research work was focused on the exploration of amphetamine adsorbents/sensors through the assessments of carbon and boron nitride graphdiyne nanosheets to reveal insights into the detection mechanism.

After the innovation of nanostructures, they have been the target of several studies to be recognized and characterized for approaching specific purposes in different fields of functions and applications [40–44]. Besides the firstly known carbon nanotube, several other nanostructures were introduced in different shapes and compositions [45–47]. For involving in the adsorption processes, the planar layer-like architectures have been found useful for providing an appropriate surface of interaction with other molecular and atomic substances [48–50]. Graphene has been the most famous layer-like nanosheets with the carbon atom composition, in which graphdiyne has been found soon after as another planar nanostructure [51–53]. Graphdiyne; which is a lattice of acetylene bond-connected benzene rings, has been found stable and its applicability for working in adsorption processes has been shown by further investigations [54–56]. Since the adsorption is the first step of a sensing process, graphdiyne has been found useful for working in sensor devices regarding both of adsorption suitability and electronic characterization [57–59]. In addition to the original carbon composition, the combination of boron and nitrogen atoms has been found suitable for the architecture of graphdiyne [60–62]. In this regard,

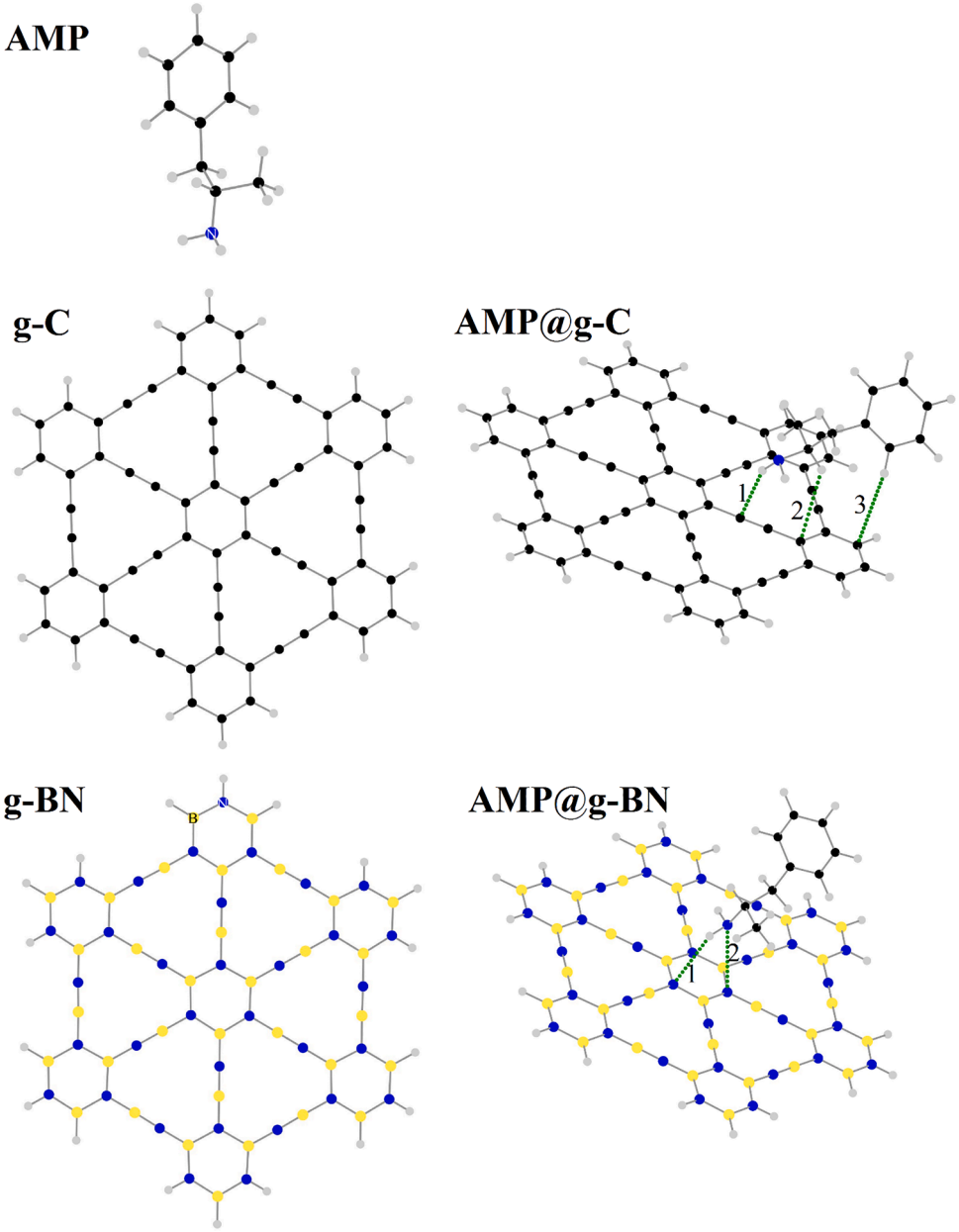

Fig. 1. Molecular representations of AMP, g-C, and g-BN Singular models and AMP@g-C and AMP@g-BN complexes; the dotted lines show the interactions.

representative models of carbon and boron nitride graphdiynes (g-C and g-BN) were assessed in the current work for sensing the amphetamine (AMP) substance along with density functional theory (DFT) calculations. The model were stabilized during the optimization calculations and their features were evaluated subsequently (Figs. 1 and 2 and Tables 1–3). To this point, the models were recognized in singular and bimolecular states for providing a molecular scale information for the adsorbing mechanism and the following sensing function based on the features structural and electronic properties. To summarize the main goal of this work, it should be mentions that adsorbents/sensors features of g-C and g-BN nanosheets were assessed for approaching insights into a facile detection of AMP substance in order to a need of emergency cares because of the serious negative impacts on human health system. This work was done at the molecular scale to reveal details of interactions between AMP and each of g-C and g-BN counterparts through the formation of AMP@g-C and AMP@g-BN complexes, in which the required information were obtained by comparing the DFT results of singular and bimolecular states.

2. Materials and methods

The current research work was done under preforming DFT calculations for optimized the structures and evaluating their features at a molecular scale study. The models were stabilized and the required features were obtained using the wB97XD/6-31G* method and basis set as implemented in the Gaussian program at the 0-charge and 1-multiplicity [63–65]. The employed level of DFT calculations was found reasonable to show the impacts of interactions on the investigating molecular systems [66]. Additionally, as we are trying to analyze the investigated systems in a comparable mode, we employed a standard basis set to approach reliable results [67]. The singular models of AMP, g-CN, and g-BN in addition to the bimolecular models of AMP@g-CN and AMP@g-BN complexes were exhibited in details. Two steps of optimizations were performed, in which the singular models were optimized first and their bimolecular models were re-optimized next. In this

Table 1
The molecular interaction features of AMP@g-C and AMP@g-BN complexes.*

Feature	AMP@g-C			AMP@g-BN	
E_{int}	-6.92			-6.51	
BSSE	1.21			2.02	
E_{int}+BSSE	-5.71			-4.49	
Interaction	1: H…C	2: H…C	3: H…C	1: H…N	2: N…N
Distance	2.98	3.31	4.29	3.05	3.51
Rho	0.0041	0.0026	0.0003	0.0038	0.0051
Del^2-Rho	0.0139	0.0079	0.0015	0.0145	0.0152
H	0.0084	0.0043	0.0012	0.0077	0.0048

* E_{int}, BSSE, and E_{int}+BSSE are in kcal/mol; Distance is in angstrom; Rho, Del^2-Rho, and H are in atomic unit.

Table 2
The frontier molecular orbital features of AMP, g-C, and g-BN singular models and AMP@g-C and AMP@g-BN complexes.*

Feature	AMP	g-C	g-BN	AMP@g-C	AMP@g-BN
HOMO	-8.43	-6.97	-8.65	-7.02	-8.35
LUMO	1.97	-1.12	1.33	-1.18	1.33
E_{gap}	10.40	5.86	9.98	5.84	9.67
C_{hard}	5.20	2.93	4.99	2.92	4.84
C_{pot}	-3.23	-4.05	-3.66	-4.10	-3.51

* All units are in eV.

Table 3
The impact of water solvent on the formation of AMP@g-C and AMP@g-BN complexes.*

Water Solvent Impact	AMP@g-C	AMP@g-BN
ΔG(Water-Gas)	-17.66	-18.94

* $\Delta G(Water\text{-}Gas) = \Delta G_{Water} - \Delta G_{Gas}$. The values are in kcal/mol.

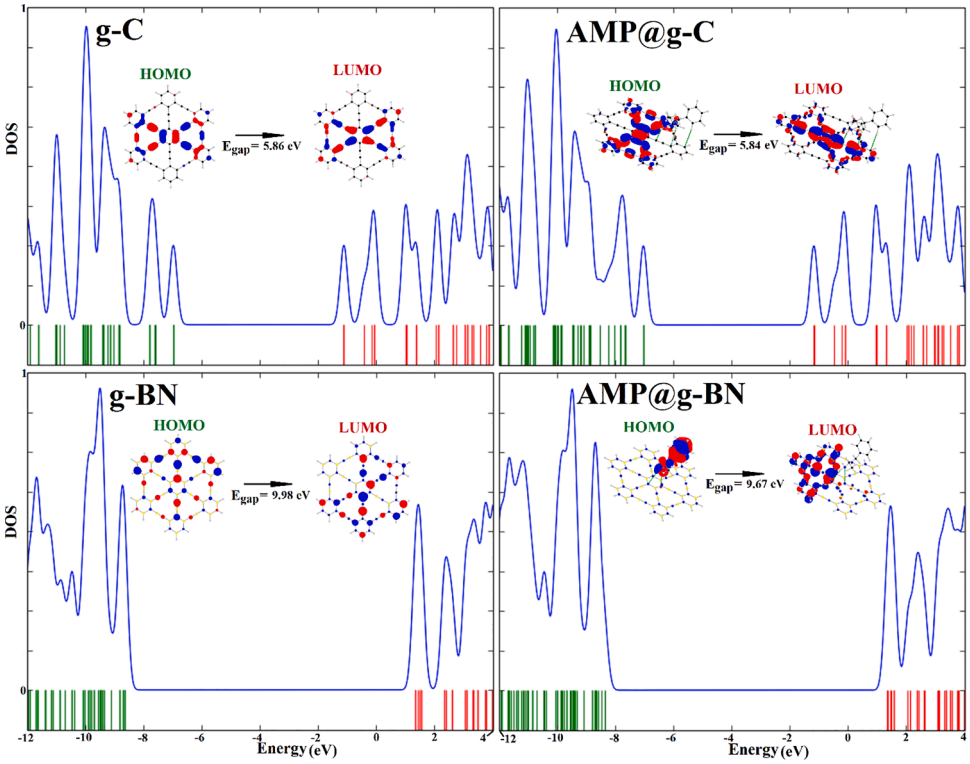

Fig. 2. HOMO-LUMO distribution patterns included DOS diagrams representations of g-C and g-BN singular models and AMP@g-C and AMP@g-BN complexes.

regard, the bimolecular models were found in a non-covalent interaction mode; hence, the original atomic stoichiometries of AMP (C_9NH_{13}) and each of g-C ($C_{66}H_{18}$) and g-BN ($B_{33}N_{33}H_{18}$) were kept unchanged in the bimolecular models. The role of hydrogen atoms were for terminating the edges of nanosheets avoiding the existence of any dangling effect for keeping the planar layer-like structure [68]. Details of interactions between the counterparts of bimolecular models were recognized by performing additional quantum theory of atoms in molecules (QTAIM) analyses [69–71], in which the results were shown by dotted lines in Fig. 1 and the corresponding quantities in Table 1. Next, the strength of interacting models were analyzed by comparing the energies of singular and bimolecular models within the interaction energy (E_{int}) values of Table 1. The effects of basis set superposition error (BSSE) [72] were considered for avoiding any overestimation E_{int} values. Subsequently, the frontier molecular orbital (FMO) analyses [73] were performed for charactering the electronic features of stabilized models, in which the results were shown by graphical representations in Fig. 2 and the corresponding quantities in Table 2. To this aim, the highest occupied molecular orbital (HOMO) and the lowest unoccupied molecular orbital (LUMO) levels were investigated in their pure levels and also their related features, in which the distribution patterns and density of states (DOS) diagrams were visualized in Fig. 2. Besides, the values of HOMO and LUMO energies, energy gap (E_{gap}), chemical hardness (C_{hard}), and chemical potential (C_{pot}) were listed in Table 2. The Multiwfn [74], GaussSum [75], and ChemCraft [76] programs were used for extracting the values and visualizations. The impact of water solvent on the formation of complexes (Table 3) was assessed using an additional polarizable continuum model (PCM) based calculations [77]. To emphasize on the importance of computational works, it could be mentioned that several scientific problems could be successfully solved by performing computational studies to obtain detailed results and information [78–80].

3. Results and discussion

Exploring amphetamine (AMP) adsorbents/sensors through the DFT assessments of carbon (g-C) and boron nitride (g-BN) graphdiyne nanosheets was done in this work. The main purpose of the current research work was indeed to explore an appropriate adsorbent for working towards the sensing function of AMP substance. The representative models of g-C and g-BN (Fig. 1) were optimized to obtain the stabilized nanosheets for adsorbing/sensing the AMP substance during the formations of AMP@g-C and AMP@g-BN complexes under the performance of re-optimization calculations. Accordingly, the stabilized models were found in the singular and bimolecular states for comparing the features of interacting substances before and after the complexations. To this aim, different starting positions of AMP towards the nanosheets were examined, in which the only meaningful one was found with the amine head of AMP for involving in interactions with both of investigated nanosheets. As a consequence, one complex was assigned as the reference model of complexation for the interaction of AMP with g-C and g-BN nanosheets shown by AMP@g-C and AMP@g-BN. The results of optimization calculations yielded the stabilized structures and their energies, in which comparing the energy values could lead to the evaluation of interaction energy (E_{int}) between the counterparts. Using Eq. (1), the values of E_{int} were evaluated and they were summarized in Table 1, in which the effects of BSSE were implemented in the E_{int} values using Eq. (2) to avoid the overestimation error. Comparing the values of E_{int} and E_{int}+BSSE could show a fixed order of strength levels of two complexes, but with a smaller values after employing the correction.

$$E_{int} = E_{Complex} - E_{AM}P - E_{Nanosheet} \quad (1)$$

$$E_{int}+BSSE = E_{Complex} - E_{AM}P - E_{Nanosheet}+BSSE \quad (2)$$

As listed in Table 1, -6.92 kcal/mol was found for the E_{int} of AMP@g-C complex and -6.51 kcal/mol was found for the E_{int} of AMP@g-BN complex, in which these values were reduced to -5.71 kcal/mol and -4.49 kcal/mol in the E_{int}+BSSE mode, respectively. Based on these results, a higher strength of interaction was found for the formation of AMP@g-C complex in comparison with the formation of AMP@g-BN complex showing a general suitability of g-C for working as stronger adsorbent of AMP substance. To learn details of this achievement, the QTAIM analyses were performed on the complexes and the results indicated the existence of three interactions in the AMP@g-C complex versus two interactions in the AMP@g-BN complex. Another point was the involvement of amine group, alkyl linker, and benzene ring of AMP in interaction with the g-C nanosheet, but the amine group of AMP was only involved in the interaction with the g-BN nanosheet. Additionally, the shortest interaction distance of AMP@g-C complex was 2.98 Å and that of AMP@g-BN complex was 3.05 Å. The values of Rho, Del^2-Rho, and H, which indicate the electron density, Laplacian of electron density, and energy density, respectively, also affirmed a significant contribution of each interaction to the complex formation. The H…C type of interaction was found in the AMP@g-C complex and the H…N and N…N interactions were found in the AMP@g-BN complex. The formation of both complexes was obtained by the involvement of physical and non-covalent interactions yielding a reusability for the nanosheets after managing the first adsorption. On the other hand, a higher strength of AMP@g-C complex could lead to a longer time of recovery for the adsorbed AMP substance in comparison with a shorter time for the AMP@g-BN complex because of a lower strength. The obtained details indicated very insightful information to learn both of mechanism of interactions between the substances and also their formation strengths regarding the main goal of this study. As a consequence, the first step of sensing function was successfully approached through the meaningful adsorptions of AMP by each of g-C and g-BN nanosheets, in which the strengths and time of recovery could be customized by employing each of AMP@g-C and AMP@g-BN complexes for the purpose.

Further assessments of sensing functions were done based on the obtained features of FMO analyses Table 2 and Fig. 2), in which the HOMO and LUMO levels were playing a dominant role of assigning these features for the investigated models. As the HOMO and LUMO levels stand for the donating and accepting levels, the obtained results indicated a difference of these levels for the singular g-C and g-BN nanosheets. Comparing the models revealed that the HOMO level of g-BN was more reachable by an energy value of -8.35 eV but the LUMO level of g-C was more reachable by an energy value of -1.18 eV. Although the values of HOMO and LUMO were calculated directly, but their derivatives including energy gap (E_{gap}), chemical hardness (C_{hard}), and chemical potential (C_{pot}) were obtained using eqs. ((3)-(5). By including these FMO features, the electronic behavior of investigated g-C and g-BN systems were assessable towards adsorbing/sensing the AMP drug substance. Additionally, comparing the quantities of different singular and complex states could reveal insights into the impacts of complex formations on the electronic features.

$$E_{gap} = LUMO - HOMO \quad (3)$$

$$C_{hard} = 1/2(LUMO - HOMO) \quad (4)$$

$$C_{pot} = 1/2(LUMO + HOMO) \quad (5)$$

The values of E_{gap} were found 5.86 eV and 9.98 eV for the singular g-C and g-BN models showing a higher rate of conductance for the g-C nanosheet in comparison with the g-BN nanosheet. Indeed, the energy distance of HOM and LUMO levels is dominant for recognizing the tendency of a molecular system for involving in the electron transferring process, in which the results indicated a higher tendency for the g-C model with a shorter energy distance than the g-BN model. To this point, the values of C_{hard} indicated a softer state for the g-C nanosheet (C_{hard} = 2.93 eV) than the g-BN nanosheet (C_{hard} = 4.99 eV) for involving in further reactions and interactions. Remembering a higher strength of

formation for the AMP@g-C complex than the AMP@g-BN complex could be described by achieving a softer g-C nanosheet. In this regard, the results were found reliable by the parallel achievements of FMO analyses and the complex strengths. Accordingly, a more suitable value of C_{pot} was obtained for the g-C nanosheet (C_{pot} = -4.05 eV) than the g-BN nanosheet (C_{pot} = -3.66 eV) to affirm the results. During the complex formations, the levels of HOMO were changed for both complexes, but the level of LUMO was remained fixed for the g-BN nanosheet and the corresponding AMP@g-BN complex. However, the energy distances of HOMO and LUMO were changed in both complexes in comparison with the singular nanosheets. To this point, a recognition process could be obtained by monitoring the changes of E_{gap} between the singular and complex states. The flexibility of g-C nanosheet for involving in interactions and reaction with other substances yielded rearrangements of both of HOMO and LUMO levels for the AMP@g-C complex whereas the HOMO level was only changed for the AMP@g-BN complex in comparison with the singular g-BN nanosheet. Hence, the change of E_{gap} between the g-C and AMP@g-C models (5.86 eV → 5.84 eV) was smaller than the change of E_{gap} between the g-BN and AMP@g-BN models (9.98 eV → 9.67 eV). This achievement could lead to detection of higher change of rate of conductance for the formation of AMP@g-BN model in comparison with that of AMP@g-C model. Accordingly, values of C_{hard} and C_{pot} quantities showed the corresponding changes during the singular to complex states conversions.

Based on the visualized distribution patterns of HOMO and LUMO (Fig. 2), it was found that the localizations of these molecular orbitals were found almost at the same place in both of singular g-C and bimolecular AMP@g-C models whereas the localizations were found at different places in singular g-BN and bimolecular AMP@g-BN models. Accordingly, the change of E_{gap} during the complex formation was found more significant for the g-BN model than the g-C model. While the localizations of molecular orbitals were found at the nanosheet side in the AMP@g-C complex, but the localizations were also found at the AMP side in the AMP@g-BN complex. This achievement could be related to a higher stability of AMP@g-C complex formation in comparison with the AMP@g-BN complex formation, in which the electronic features were found in complimentary to the structural features. Recording the variation of other molecular orbital levels behind the HOMO level and next to the LUMO levels was done along with the DOS diagrams, in which the results indicated possibility of complex formation detection by these diagrams. Accordingly, a sensor function could be found for the g-C and g-BN nanosheets towards the AMP substance.

The impact of water solvent on the formation of AMP@g-C and AMP@g-BN complexes was investigated by calculating the Gibbs free energy (G) quantities of complexes in gas and water phase, then comparing the results to obtain ΔG(Water-Gas). The results indicated a suitability of water solvent for the formation of complexes by indicating the values of -17.66 kcal/mol and -18.94 kcal/mol for AMP@g-C and AMP@g-BN complexes, respectively. Additionally, by providing a hetero-atomic surface, the formation of AMP@g-BN complex was found even better than the formation of AMP@g-C complex. As a consequence, both complexes could be available in the water solvent phase with a priority of AMP@g-BN complex.

It should be mentioned here that the expected adsorbing/sensing function is supposed to work at a traceless concentration of AMP especially in the exhaled berating air, then small changes could be expected for the detector devices. Hence, a successful adsorbing/sensing function could be found for both of g-C and g-BN nanosheets towards the AMP substance, in which the g-BN nanosheet could be proposed for a rapid detection and the g-C nanosheet could be proposed for a timely detection. In the other words, the availability of AMP@g-C complex was found longer than that of AMP@g-BN complex making possible its delivery to a second detector device by time whereas the AMP@g-BN complex should be detected immediately. Additionally, the g-BN nanosheet was found more reusable than the g-C nanosheet for the purpose of a longer working life of a sensor material. As an important issue regarding the possibility of toxicity of nanostructures for working in the biological related systems, developing non-invasive platforms could be very helpful for solving that challenging issue as was done in the current work. As a concluding remark, both of g-C and g-BN could be employed as adsorbents/sensors of AMP substance, in which the using conditions could customize them for the targeted application.

4. Conclusions

Exploring AMP adsorbents/sensors through the DFT assessments of g-C and g-BN nanosheets were done in this work regarding the importance of providing facile detention process of toxic substances for the emergency health activities. The models were optimized and their features were obtained for recognizing the investigated models under the evaluated structural and electronic specifications. The g-C and g-BN nanosheets provided a suitable surface for the AMP substance to interact with each other in a non-covalent mode resulting a higher strength for the AMP@g-C complex than the AMP@g-BN complex. However, the variation of E_{gap} values during the complex formation was more significant for the AMP@g-BN complex. The adsorption features indicated a longer time of availability for the AMP@g-C complex than the AMP@g-BN complex making a possibility of timely detection for the AMP@g-C complex; however, an immediately detection was needed for the AMP@g-BN complex. Monitoring the variations of molecular orbital features also indicated possibility of detention processes for the formation of both complexes, in which a customization could be done for approaching a desired function. Moreover, the water solvent showed a better suitability of formation for the AMP@g-BN complex prior to the AMP@g-C complex. As a final result of this work, the investigated g-C and g-BN nanosheets were found suitable for managing a successful adsorbing/sensing function towards the AMP substance bases on the characteristic structural and electronic fealties, which makes them to be used in a customized process.

CRediT authorship contribution statement

M.J. Saadh: Conceptualization, Investigation, Writing – original draft. **S.M. Mohealdeen:** Conceptualization, Data curation, Validation, Writing – review & editing. **C.Y. Hsu:** Formal analysis, Investigation, Writing – review & editing. **U.A. Jumanazarov:** Writing – review & editing. **R.R. Maaliw:** Formal analysis, Visualization. **M. Mirzaei:** Investigation, Methodology, Writing – original draft. **M. Da'i:** Investigation, Validation. **K. Harismah:** Conceptualization, Methodology, Supervision.

Declaration of Competing Interest

The authors declare that they have no known competing financial interests or personal relationships that could have appeared to influence the work reported in this paper.

Data availability

Data will be made available on request.

References

[1] A. John, L. Benny, A.R. Cherian, S.Y. Narahari, A. Varghese, G. Hegde, Electrochemical sensors using conducting polymer/noble metal nanoparticle nanocomposites for the detection of various analytes: a review, J. Nanostructure Chem. 11 (2021) 1.
[2] S. Ariavand, M. Ebrahimi, E. Foladi, Design and construction of a novel and an efficient potentiometric sensor for determination of sodium ion in urban water samples, Chem. Methodol. 6 (2022) 886.
[3] M.N. Awan, H. Razzaq, O.U. Abid, S. Qaisar, Recent advances in electroanalysis of hydrazine by conducting polymers nanocomposites: a review, J. Chem. Rev. 5 (2023) 311.

[4] A. Farooq, A.B. Alquaity, M. Raza, E.F. Nasir, S. Yao, W. Ren, Laser sensors for energy systems and process industries: perspectives and directions, Prog. Energy Combust. Sci. 91 (2022), 100997.
[5] T. Tarmuji, Perancangan dan pembuatan alat pengukur getaran mekanis menggunakan piezzo electric sensor berbasis arduino mikrokontroller, Emit. J. Tek. Elektro 15 (2015) 53.
[6] M. Mirzaei, A.H. Rasouli, A. Saedi, HOMO-LUMO photosensitization analyses of coronene-cytosine complexes, Main Group Chem. 20 (2021) 565.
[7] B. Sumanto, M. Fakhrurrifqi, Utilization of gas sensor array and principal component analysis to identify fish decomposition level, Khazanah Informatika: Jurnal Ilmu Komputer dan Informatika 6 (2020) 190.
[8] E. Sharifi Pour, M. Ebrahimi, H. Beitollai, Electrochemical sensing of theophylline using modified glassy carbon electrode, Chem. Methodol. 6 (2022) 560.
[9] V. Safari Fard, Y. Davoudabadi Farahani, An amine/imine functionalized microporous MOF as a new fluorescent probe exhibiting selective sensing of Fe3+ and Al3+ over mixed metal ions, J. Appl. Organomet. Chem. 2 (2022) 165.
[10] I. Patra, F. H. Mohammed, A.K.O. Aldulaimi, D. Abbas khudhair, Y. Fakri Mustafa, A novel and efficient magnetically recoverable copper catalyst [MNPs-guanidine-bis (ethanol)-Cu] for Pd-free Sonogashira coupling reaction, Synth. Commun. 52 (2022) 1856.
[11] A.A. Peyghan, H. Soleymanabadi, Adsorption of H2S at Stone–Wales defects of graphene-like BC3: a computational study, Mol. Phys. 112 (2014) 2737.
[12] H. Salimi, A. Ahmadi Peyghan, M. Noei, Adsorption of formic acid and formate anion on ZnO nanocage: a DFT study, J. Cluster Sci. 26 (2015) 609.
[13] M. Giahi, M. Mirzaei, G. Veghar Lahijani, Potentiometric PVC membrane sensor for the determination of phenylephrine hydrochloride in some pharmaceutical products, J. Iran. Chem. Soc. 7 (2010) 333.
[14] E. Golipour-Chobar, F. Salimi, G. Ebrahimzadeh-Rajaei, Sensing of lomustine drug by pure and doped C48 nanoclusters: DFT calculations, Chem. Methodol. 6 (2022) 790.
[15] H. Roshanfekr, A simple specific dopamine aptasensor based on partially reduced graphene oxide–AuNPs composite, Prog. Chem. Biochem. Res. 6 (2023) 61.
[16] R.F. Kranenburg, F. Ou, P. Sevo, M. Petruzzella, R. de Ridder, A. van Klinken, K. D. Hakkel, D.M. van Elst, R. van Veldhoven, F. Pagliano, AC. van Asten, On-site illicit-drug detection with an integrated near-infrared spectral sensor: a proof of concept, Talanta 245 (2022), 123441.
[17] O. Özbek, C. Berkel, Ö. Isildak, Applications of potentiometric sensors for the determination of drug molecules in biological samples, Crit. Rev. Anal. Chem. 52 (2022) 768.
[18] D. Olegovich Bokov, A.T. Jalil, F.H. Alsultany, M.Z. Mahmoud, W. Suksatan, S. Chupradit, M.T. Qasim, P. Delir Kheirollahi Nezhad, Ir-decorated gallium nitride nanotubes as a chemical sensor for recognition of mesalamine drug: a DFT study, Mol. Simul. 48 (2022) 438.
[19] D.J. Heal, S.L. Smith, J. Gosden, DJ. Nutt, Amphetamine, past and present–a pharmacological and clinical perspective, J. Psychopharmacol. 27 (2013) 479.
[20] K.Y. O'Malley, C.L. Hart, S. Casey, LA. Downey, Methamphetamine, amphetamine, and aggression in humans: a systematic review of drug administration studies, Neurosci. Biobehav. Rev. 141 (2022), 104805.
[21] M. Heikkinen, H. Taipale, A. Tanskanen, E. Mittendorfer-Rutz, M. Lähteenvuo, J. Tiihonen, Association of pharmacological treatments and hospitalization and death in individuals with amphetamine use disorders in a Swedish Nationwide cohort of 13965 patients, JAMA Psychiatry 80 (2023) 31.
[22] K.J. Siefried, L.S. Acheson, N. Lintzeris, N. Ezard, Pharmacological treatment of methamphetamine/amphetamine dependence: a systematic review, CNS Drugs 34 (2020) 337.
[23] A.C. Childress, M. Komolova, FR. Sallee, An update on the pharmacokinetic considerations in the treatment of ADHD with long-acting methylphenidate and amphetamine formulations, Expert Opin. Drug Metab. Toxicol. 15 (2019) 937.
[24] Ș. Stăcescu, G. Hancu, D. Podar, Ș. Todea, A. Tero-Vescan, A historical overview upon the use of amphetamine derivatives in the treatment of obesity, J. Pharm. Care 7 (2019) 72.
[25] J. Berezanskaya, W. Cade, T.M. Best, K. Paultre, C. Kienstra, ADHD prescription medications and their effect on athletic performance: a systematic review and meta-analysis, Sports Med. Open 8 (2022) 1.
[26] M. Morelli, E. Tognotti, Brief history of the medical and non-medical use of amphetamine-like psychostimulants, Exp. Neurol. 342 (2021), 113754.
[27] FM. Kassim, Systematic reviews of the acute effects of amphetamine on working memory and other cognitive performances in healthy individuals, with a focus on the potential influence of personality traits, Hum. Psychopharmacol.: Clin. Exp. 38 (2023) e2856.
[28] A.M. Vivolo-Kantor, B.E. Hoots, P. Seth, C.M. Jones, Recent trends and associated factors of amphetamine-type stimulant overdoses in emergency departments, Drug Alcohol Depend. 216 (2020), 108323.
[29] R.S. Alharbi, A.H. Alhowail, A.G. Alharbi, A.M. Emara, Evaluation of the health status outcome among inpatients treated for amphetamine addiction, Saudi J. Biol. Sci. 29 (2022) 1465.
[30] J. Shakeri, S.M. Ahmadi, F. Maleki, M.R. Hesami, A.P. Moghadam, A. Ahmadzade, M. Shirzadi, A. Elahi, Effectiveness of group narrative therapy on depression, quality of life, and anxiety in people with amphetamine addiction: a randomized clinical trial, Iran. J. Med. Sci. 45 (2020) 91.
[31] J.R. Richards, T.W. Placone, C.G. Wang, M.C. van der Linden, R.W. Derlet, EG. Laurin, Methamphetamine, amphetamine, and MDMA use and emergency department recidivism, J. Emerg. Med. 59 (2020) 320.
[32] M. Gerdtz, C.Y. Yap, C. Daniel, J.C. Knott, P. Kelly, A. Innes, G. Braitberg, Amphetamine-type stimulant use among patients admitted to the emergency department behavioural assessment unit: screening and referral outcomes, Int. J. Ment. Health Nurs. 29 (2020) 796.
[33] B.M. Chivaurah, D. Lienert, D. Coates, Amphetamine-type-substance-related presentations to the emergency department mental health team of a local health district in Australia, Australas Psychiatry 27 (2019) 369.
[34] H. Bano, S. Suleman, N. Anzar, S. Parvez, J. Narang, A review on advancement of biosensors for the detection of amphetamine drug, Int. J. Environ. Anal. Chem. (2023).
[35] F. Xu, J. Zhou, H. Yang, L. Chen, J. Zhong, Y. Peng, K. Wu, Y. Wang, H. Fan, X. Yang, Y. Zhao, Recent advances in exhaled breath sample preparation technologies for drug of abuse detection, TrAC Trends Anal. Chem. 157 (2022), 116828.
[36] K. Brown, L. Dennany, Electrochemical devices for forensic chemical sensing, Forensic Anal. Methods 13 (2019) 115.
[37] S. Alizadeh, Z. Nazari, Amphetamine, methamphetamine, morphine @ AuNPs kit based on PARAFAC, Adv. J. Chem. A 5 (2022) 253.
[38] N.F. Montiel, M. Parrilla, N. Sleegers, F. Van Durme, A.L. van Nuijs, K. De Wael, Electrochemical sensing of amphetamine-type stimulants (pre)-precursors to fight against the illicit production of synthetic drugs, Electrochim. Acta 436 (2022), 141446.
[39] F. Truta, A.G. Cruz, M. Tertis, C. Zaleski, G. Adamu, N.S. Allcock, M. Suciu, M. G. Ștefan, B. Kiss, E. Piletska, K. De Wael, NanoMIPs-based electrochemical sensors for selective detection of amphetamine, Microchem. J. 191 (2023), 108821.
[40] N. Ngafwan, I.N. Wardana, W. Wijayanti, E. Siswanto, The role of NaOH and papaya latex bio-activator during production of carbon nanoparticle from rice husks, Adv. Nat. Sci.: Nanosci. Nanotechnol. 9 (2018), 045011.
[41] N. Ngafwan, H. Rasyid, E.S. Abood, W.K. Abdelbasset, Al-S SG, D. Bokov, AT. Jalil, Study on novel fluorescent carbon nanomaterials in food analysis, Food Sci. Technol. 42 (2021) e37821.
[42] A. Jimoh, S. Uba, V. Ajibola, E. Agbaji, Effect of nanoparticles on the degradation, ageing and other properties of ester-based nanofluids, Adv. J. Chem. A 6 (2023) 105.
[43] F. Banifatemeh, Polymerization of graphite and carbon compounds by aldol condensation as anti-corrosion coating, Asian J. Green Chem. 7 (2023) 25.
[44] A.K.O. Aldulaim, N. M Hameed, T. Ahmed Hamza, A. S Abed, The antibacterial characteristics of fluorescent carbon nanoparticles modified silicone denture soft liner, J. Nanostructures 12 (2022) 774.
[45] M. Nasrollahzadeh, Z. Issaabadi, M. Sajjadi, S.M. Sajadi, M. Atarod, Types of nanostructures, Interface Sci. Technol. 28 (2019) 29.
[46] N. Farhami, A computational study of thiophene adsorption on boron nNitride nanotube, J. Appl. Organomet. Chem. 2 (2022) 148.
[47] H. Peyman, Design and fabrication of modified DNA-Gp nano-biocomposite electrode for industrial dye measurement and oOptical confirmation, Prog. Chem. Biochem. Res. 5 (2022) 391.
[48] F. Zhang, K. Yang, G. Liu, Y. Chen, M. Wang, S. Li, R. Li, Recent advances on graphene: synthesis, properties and applications, Compos. A 160 (2022), 107051.
[49] C. Li, C. Zheng, F. Cao, Y. Zhang, X. Xia, The development trend of graphene derivatives, J. Electron. Mater. 51 (2022) 4107.
[50] S. Pour Karim, R. Ahmadi, M. Yousefi, K. Kalateh, G. Zarei, Interaction of graphene with amoxicillin antibiotic by in silico study, Chem. Methodol. 6 (2022) 861.
[51] AK. Geim, Graphene: status and prospects, Science 324 (2009) 1530.
[52] X. Gao, H. Liu, D. Wang, J. Zhang, Graphdiyne: synthesis, properties, and applications, Chem. Soc. Rev. 48 (2019) 908.
[53] Y. Fang, Y. Liu, L. Qi, Y. Xue, Y. Li, 2D graphdiyne: an emerging carbon material, Chem. Soc. Rev. 51 (2022) 2681.
[54] X. Zheng, S. Chen, J. Li, H. Wu, C. Zhang, D. Zhang, X. Chen, Y. Gao, F. He, L. Hui, H. Liu, Two-dimensional carbon graphdiyne: Advances in fundamental and application research, ACS Nano 17 (2023) 14309.
[55] G. Yang, Z. Li, S. Wang, J. Lin, Achieving high quantum capacitance graphdiyne through doping and adsorption, Phys. Chem. Chem. Phys. 25 (2023) 2012.
[56] H. Ma, B.B. Yang, Z. Wang, K. Wu, C. Zhang, A three dimensional graphdiyne-like porous triptycene network for gas adsorption and separation, RSC Adv. 12 (2022) 28299.
[57] X. Li, Y. Zheng, W. Wu, M. Jin, Q. Zhou, L. Fu, N. Zare, F. Karimi, M. Moghadam, Graphdiyne applications in sensors: a bibliometric analysis and literature review, Chemosphere 307 (2022), 135720.
[58] Y. Cai, J. Shen, J.H. Fu, N. Qaiser, C. Chen, C.C. Tseng, M. Hakami, Z. Yang, H. J. Yen, X. Dong, L.J. Li, Graphdiyne-based nanofilms for compliant on-skin sensing, ACS Nano 16 (2022) 16677.
[59] J. Li, C. Wan, C. Wang, H. Zhang, X. Chen, 2D material chemistry: graphdiyne-based biochemical sensing, Chem. Res. Chin. Univ. 36 (2020) 622.
[60] J. Hou, L. Sun, Q. Pan, Y. Zhao, Recent synthetic methods towards graphdiyne, ChemNanoMat 9 (2023), e202300273.
[61] Z. Yang, Y. Zhang, M. Guo, J. Yun, Adsorption of hydrogen and oxygen on graphdiyne and its BN analog sheets: a density functional theory study, Comput. Mater. Sci. 160 (2019) 197.
[62] N. Hou, X.H. Fang, R. Feng, DFT study of the influence of boron/nitrogen substitution on the electronic and nonlinear optical properties of the benzene-substituted graphdiyne fragment, Comput. Theor. Chem. 1209 (2022), 113629.
[63] J.D. Chai, M. Head-Gordon, Long-range corrected hybrid density functionals with damped atom–atom dispersion corrections, Phys. Chem. Chem. Phys. 10 (2008) 6615.
[64] V.A. Rassolov, M.A. Ratner, J.A. Pople, P.C. Redfern, LA. Curtiss, 6-31G* basis set for third-row atoms, J. Comput. Chem. 22 (2001) 976.
[65] M.J. Frisch, G.W. Trucks, H.B. Schlegel, G.E. Scuseria, M.A. Robb, J.R. Cheeseman, et al., Gaussian 09 program, Gaussian Inc, Wallingford, CT, 2009.

[66] S. Tsuzuki, T. Uchimaru, Accuracy of intermolecular interaction energies, particularly those of hetero-atom containing molecules obtained by DFT calculations with Grimme's D2, D3 and D3BJ dispersion corrections, Phys. Chem. Chem. Phys. 22 (2020) 22508.
[67] E.C. Garrett, AS. Serianni, Ab initio molecular orbital calculations on furanose sugars: a study with the 6-31G basis set, Carbohydr. Res. 206 (1990) 183.
[68] M. Mirzaei, O. Gulseren, DFT studies of CNT–functionalized uracil-acetate hybrids, Phys. E 73 (2015) 105.
[69] R.F. Bader, TT. Nguyen-Dang, Quantum theory of atoms in molecules–Dalton revisited, Adv. Quantum Chem. (1981) 14.
[70] A. Parkan, M. Mirzaei, N. Tavakoli, A. Homayouni, Molecular interactions of indomethacin and amino acids: computational approach, Main Group Chem. 21 (2022) 611.
[71] M. Ghiasifar, T. Hosseinnejad, A. Ahangar, Copper catalyzed cycloaddition reaction of azidomethyl benzene with 2,2-di(prop-2-yn-1-yl)propane-1,3-diol: DFT and QTAIM investigation, Prog. Chem. Biochem. Res. 5 (2022) 1.
[72] E.R. Davidson, SJ. Chakravorty, A possible definition of basis set superposition error, Chem. Phys. Lett. 217 (1994) 48.
[73] M. Solimannejad, M. Noormohammadbeigi, Boron nitride nanotube (BNNT) as a sensor of hydroperoxyl radical (HO2): a DFT study, J. Iran. Chem. Soc. 14 (2017) 471.
[74] T. Lu, F. Chen, Multiwfn: A multifunctional wavefunction analyzer, J. Comput. Chem. 33 (2012) 580.
[75] N.M. O'boyle, A.L. Tenderholt, KM. Langner, Cclib: a library for package-independent computational chemistry algorithms, J. Comput. Chem. 29 (2008) 839.
[76] Chemcraft - graphical software for visualization of quantum chemistry computations. Version 1.8, build 654. https://www.chemcraftprog.com.
[77] B. Mennucci, Polarizable continuum model, Wiley Interdiscip. Rev.: Comput. Mol. Sci. 2 (2012) 386.
[78] F. Toiserkani, M. Mirzaei, V. Alcan, K. Harismah, M.M. Salem-Bekhit, A facile detection of ethanol by the Be/Mg/Ca-enhanced fullerenes: Insights from density functional theory, Chem. Phys. Impact 7 (2023), 100318.
[79] M. Da'i, M. Mirzaei, F. Toiserkani, S.M. Mohealdeen, Y. Yasin, M.M. Salem-Bekhit, R. Akhavan-Sigari, Sensing the formaldehyde pollutant by an enhanced BNC18 fullerene: DFT outlook, Chem. Phys. Impact 7 (2023), 100306.
[80] M.N. Sidik, Y.M. Bakri, S.S. Azziz, A.K.O. Aldulaimi, C.F. Wong, M. Ibrahim, In silico xanthine oxidase inhibitory activities of alkaloids isolated from Alphonsea sp, S. Afr. J. Bot. 147 (2022) 820.